Remote energetic neutral atom imaging of electric potential over a lunar magnetic anomaly

Y. Futaana,[1] S. Barabash,[1] M. Wieser,[1] C. Lue,[1,2] P. Wurz,[3] A. Vorburger,[3] A. Bhardwaj,[4] and K. Asamura[5]

Received 30 October 2012; revised 27 December 2012; accepted 30 December 2012; published 31 January 2013.

[1] The formation of electric potential over lunar magnetized regions is essential for understanding fundamental lunar science, for understanding the lunar environment, and for planning human exploration on the Moon. A large positive electric potential was predicted and detected from single point measurements. Here, we demonstrate a remote imaging technique of electric potential mapping at the lunar surface, making use of a new concept involving hydrogen neutral atoms derived from solar wind. We apply the technique to a lunar magnetized region using an existing dataset of the neutral atom energy spectrometer SARA/CENA on Chandrayaan-1. Electrostatic potential larger than +135 V inside the Gerasimovic anomaly is confirmed. This structure is found spreading all over the magnetized region. The widely spread electric potential can influence the local plasma and dust environment near the magnetic anomaly.
Citation: Futaana, Y., S. Barabash, M. Wieser, C. Lue, P. Wurz, A. Vorburger, A. Bhardwaj, and K. Asamura (2013), Remote energetic neutral atom imaging of electric potential over a lunar magnetic anomaly, *Geophys. Res. Lett.*, *40*, 262–266, doi:10.1002/grl.50135.

1. Introduction

[2] The electrostatic potential between the Moon surface and space is a key parameter that is fundamental for lunar science and human exploration on the Moon. Many investigations of electric potential and associated electric fields have been conducted from the surface using solar wind plasma since the Apollo era. Surface potential influences ambient plasma characteristics and electric current, which balances each other to produce an equilibrium state [*Whipple*, 1981]. A large electric potential, sometimes less than 1 kV, was found from electron energy spectra when high-energy electrons precipitated onto the lunar surface [*Halekas et al*., 2005]. The resulting induced current may potentially damage lander components. The surface potential also affects the environment by influencing dust dynamics and vice versa [e.g., *Nitter et al*., 1998; *Stubbs et al*., 2011; *Garrick-Bethell et al*., 2011].

[3] On the other hand, a positive potential is not generally very large. For example, *Freeman et al*. [1973] used in situ measurement of suprathermal ions and found approximately +10V surface potential. *Goldstein* [1974] used electron data to find the −3 to +5V potential. These results are consistent with theoretical predictions of a few to +20V [e.g., *Freeman and Ibrahim*, 1975]. The exception has been found inside the local magnetized regions (magnetic anomalies) on the lunar surface [e.g., *Barnes et al*., 1971; *Hood et al*., 1979; *Tsunakawa et al*., 2010], where a positive electric potential of the order of ~100 V is expected [*Saito et al*., 2012]. Such electric potentials modify the local plasma environment significantly near the anomaly. Evaluating the electrostatic environment near magnetic anomalies is important as a possible candidate of landing site for future lander missions where cosmic ray protections are expected.

[4] Energetic neutral atoms (ENAs), neutral atoms with energies more than 10 eV, have been used for diagnostics for plasma and neutral environments. The powerful remote sensing technique has provided the diagnostics with spatial scales from planetary bodies [*Futaana et al*., 2011] to the Solar System [*McComas et al*., 2012]. In the case of the Moon, the lack of an intrinsic magnetic field [*Colburn et al*., 1967; *Dyal et al*., 1974] allows the solar wind to interact directly with the surface, where ENAs are produced. Thus, ENAs provide information about the solar wind access at the lunar surface [*Futaana et al*., 2006]. The lunar ENAs have already been detected by the ENA sensor, CENA (Chandrayaan-1 Energetic Neutral Atoms), on board a lunar orbiter, Chandrayaan-1 [*Barabash et al*., 2009]. These ENAs, composed only of hydrogen, are originally solar wind protons, which are neutralized on and backscattered from the lunar surface [*Wieser et al*., 2009].

[5] The physical mechanism of the backscattered ENA generation at the lunar surface is not fully understood. The biggest unknown is what causes the high backscattering fraction of 10–20% of impinging solar wind proton flux [*Wieser et al*., 2009; *McComas et al*., 2009; *Rodríguez et al*., 2012; *Futaana et al*., 2012]. The observations contradict with classical understandings of full (<0.1%) absorption [e.g., *Behrisch and Wittmaack*, 1991; *Feldman et al*., 2000; *Crider and Vondrak*, 2002] because of the high porosity of the surface. Another unexplained signature is the ENA energy spectrum. The observed energy spectrum of the backscattered ENAs follows the Maxwell-Boltzmann distribution function with the characteristic energy, i.e., the temperature of the distribution, ranging from 60 to 140 eV. A Maxwell-Boltzmann distribution implies a state of thermal equilibrium, but it is unrealistic to assume equilibrium with such a high temperature (100 eV corresponds to 1.16×10^6 K) at the surface. Moreover, the characteristic energy depends only on the solar wind

[1]Swedish Institute of Space Physics, Kiruna, Sweden.
[2]Department of Physics, Umeå University, Umeå, Sweden.
[3]Physikalisches Institut, University of Bern, Bern, Switzerland.
[4]Space Physics Laboratory, Vikram Sarabhai Space Center, Trivandrum, India.
[5]Institute of Space and Astronautical Science, Sagamihara, Japan.

Corresponding author: Y. Futaana, Swedish Institute of Space Physics, Box 812, SE-98128 Kiruna, Sweden. (futaana@irf.se)

0094-8276/13/10.1002/grl.50135

energy; actually, the observation exhibits a linear correlation with the solar wind velocity [*Futaana et al*., 2012]. From classical theory of elastic scattering [e.g., *Niehus et al*., 1993], linearity with the incident energy (i.e., the solar wind energy) is expected. From these perspectives, an adaption of laboratory knowledge and theoretical understandings of the backscattered process to the situation of a regolith surface in space is needed.

[6] Even though the observed characteristics of the backscattered ENAs are not yet fully explained by present theory, we propose here a new empirical method to derive the lunar surface potential from observed hydrogen ENA energy spectra. In this paper, we first describe a new method to map the surface electrostatic potential. Then, we apply this method to available observations near a magnetic anomaly to show a large potential generation over a wide range of the magnetic anomaly. We also discuss the result and its influence on surface plasma and dust environments and human activities.

2. Mapping Method of Electric Potential

[7] Assuming the existence of a surface potential ($\pm\Phi_{surf}$) between the lunar surface and space (solar wind), the solar wind will be decelerated (or accelerated) before reaching the surface. The solar wind energy at the surface becomes $Esurf = Esw - (\pm\Phi_{surf})$, where *Esw* is the original solar wind energy. When the decelerated (or accelerated) solar wind is backscattered as ENAs, the generated ENA temperature, *Tena*, is determined only from the solar wind energy at the lunar surface, *Esurf* [*Futaana et al*., 2012]. Because *Tena* is a measurable quantity, we can determine *Esurf*. The difference between *Esurf* and *Esw* provides the surface potential, $\pm\Phi_{surf}$.

[8] For this method, it is important to produce a proper reference model, i.e., the relationship between *Esw* and *Tena* for uncharged surface. We here use a model derived from more than 100 CENA observations in the equatorial region [*Futaana et al*., 2012]:

$$Tena = Vsw \times 0.273 - 1.99$$

where *Tena* is measured in eV and *Vsw* is the solar wind velocity in km/s. This can be rewritten as

$$Esw = \frac{(Tena + 1.99)^2}{14.19} \quad (1)$$

where *Esw* is also measured in eV. This reference model is derived empirically. No theoretical assurance is yet provided. Here we estimated a statistical uncertainty using the dataset in *Futaana et al*. [2012] and calculated the ambiguity of the current reference model (equation (1)) to be −45 and +35 eV (as 25% and 75% percentiles, respectively). Note that the reference model is made using the nominal dayside measurements near the equator. Because no strong magnetic anomalies exist near the equator, the reference model is not affected by magnetic anomalies. On the other hand, the reference model does not account for the surface potential in the nominal dayside conditions. In the nominal dayside, the ultraviolet and electron illumination on the surface produces a potential of a few eV [*Vondrak*, 1983; *Němeček et al*., 2011]. We assume in the following analysis that the surface potential in the nominal state is negligible compared with that in the magnetic anomaly. Our results show that this assumption is realistic.

[9] This new method relies on only the energy spectrum of ENAs. Therefore, it complements classical methods using energy spectra of charged particles. Advantageously, the new method provides an electrostatic potential map. Obviously, when a proper reference model is found, this method can be applied to other airless bodies as Mercury, asteroids and Galileo moons.

3. Application to Magnetized Region

[10] We applied the above-described electric potential mapping method to the region over a lunar magnetic anomaly called Gerasimovic (Figure 1a). While there are many magnetized regions on the Moon [*Tsunakawa et al*., 2010], the Gerasimovic is an isolated anomaly, and therefore, it is suitable for a dedicated analysis and discussion [*Vorburger et al*., 2012]. We used the data obtained from the CENA sensor on the Chandrayaan-1 spacecraft over eight non-consecutive orbits from 16 June (22:06) to 18 June (00:28) 2009. The Moon was located in the solar wind. From WIND/SWE observations, the solar wind was stable (density was ~6 cm^{-3} and the velocity was ~300 km s^{-1}).

[11] As seen in the ENA flux map (Figure 1b), there are three characteristic regions [*Wieser et al*., 2010] from the ENA flux (a) outside the anomaly, (b) enhanced region, and (c) inside the anomaly. Outside the anomaly, the ENA flux depends on, to the first order, the cosine of the solar zenith angle, as the solar wind flux at the surface does. It corresponds to the drops in ENA flux at high latitudes (Figure 1b). For the electrostatic potential map (Figure 1a), a clear signature with a positive potential of >150 V is found inside the anomaly. The potential structure spread over the majority of the magnetized area. In contrast, in the enhanced region and outside the anomaly, no potential structures were found. Small-scale potential structures (below −100 or above 100 V) are most likely artificial, because the spatial scale of them is comparable to the dimension of the sensor FOV projection (~1° in latitude and ~8° in longitude).

[12] Outside the anomaly, the characteristic energy of backscattered ENA is 84.3eV (Figure 2). Using the reference model (equation (1)), the corresponding solar wind energy is found to be 525 eV. In the enhanced region, the ENA flux is higher than in the other regions, and the ENA temperature inside the enhanced region does not change (83.3 eV), indicating that the solar wind energy at the surface of the enhanced region is 512 eV. Inside the magnetic anomaly, the ENA characteristic energy is 72.5 eV, and the derived solar wind energy at the surface is 390 eV. The difference in the solar wind energy between the outside (525 eV) and inside of the anomaly (390 eV) is 135 eV, which corresponds to the deceleration of the solar wind by electrostatic potential above the magnetic anomaly.

[13] The feature of above energy spectra, namely, lower characteristic energy above magnetized region, is commonly seen in the CENA dataset. Therefore, this empirical method of electric potential derivation could also work for other magnetic anomalies, in which the surfaces are positively charged.

4. Discussion

[14] The positive potential formed above a magnetic anomaly is expected based on the charge separation theory. Ions can penetrate farther than electrons in the interaction

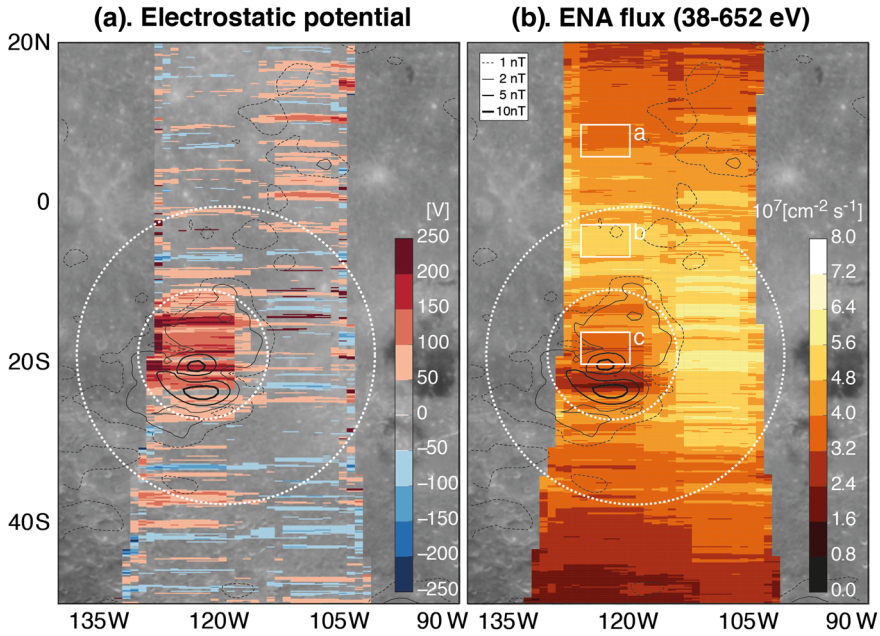

Figure 1. (a) Map of the electrostatic potential near the Gerasimovic magnetic anomaly. Color scale shows the electrostatic potential with respect to the solar wind. Two dashed circles separate the regions inside magnetic anomaly, the enhanced region, and the region outside the anomaly. (b) Map of the ENA flux integrated over 38–652 eV. Similar to the signatures in the integral flux over 150–600 eV reported previously [*Wieser et al.*, 2010], three regions can be distinctly identified. Labeled white boxes indicate the areas that produce the energy spectra shown in Figure 2. The Moon images are from the Clementine grayscale albedo map [*Archinal et al.*, 2005]. The contour lines represent the strength of the modeled magnetic field of anomalies at 30 km altitude [*Purucker and Nicholas*, 2010].

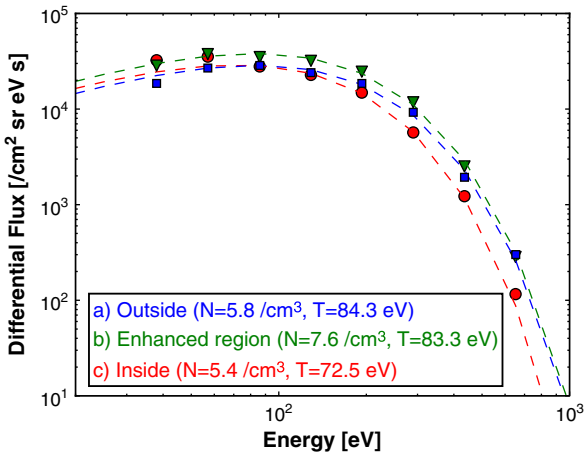

Figure 2. Energy spectra of the backscattered ENAs from three characteristic regions. The blue, green, and red lines correspond to the backscattered ENAs from (a) outside the anomaly, (b) the enhanced region, and (c) inside the anomaly, respectively (Figure 1b). The symbols show the flux observed by the CENA sensor for each region, and the dashed lines illustrate the best fit by the Maxwell-Boltzmann distributions.

region, and the charge separation produces an outward-facing electric field. Recently, *Saito et al.* [2012] demonstrated that the in situ measurements of the energy spectra for solar wind protons, alpha particles, and electrons at 30 km altitude are consistently explained if one assumes the presence of a +150 V electric potential inside the magnetic anomaly. These authors analyzed a different anomaly (South Pole Aitken), but their electric potential is in a good agreement with our result of 135 V electric potential formation.

[15] We emphasize here that we do not see any strong electric potential in the enhanced region of the magnetic anomaly. The enhanced region can be attributed to an increase in the solar wind proton flux at the lunar surface caused the deflection of the ion flow above the magnetic anomaly [*Wieser et al.*, 2010]. The deflection magnifies the net solar wind flux of the enhanced region, similar to the Earth's magnetosheath. However, the lack of electrostatic potential in the enhanced region indicates that there is no electric potential formed above the enhanced region. Therefore, the deflection above the anomaly is mainly caused by magnetic forces, and the previously suggested mini-scale bow shock [*Lin et al.*, 1998] is evidently not formed above the magnetic anomaly.

[16] The large electric potential influences the near-surface environment near the magnetic anomaly. It explains the observed signatures of solar wind ion reflection that are correlated with the magnetic anomaly [*Lue et al.*, 2011]. A high electric potential not only decelerates the incoming solar wind protons but also thermalizes the plasma and partially reflects the protons [*Saito et al.*, 2012] as illustrated in Figure 3. This also modifies the lunar dust environment because charged dust particles are lifted and transported by this large electric potential. Recently, the differentiation of dust by a large electric potential was proposed [*Garrick-Bethell et al.*, 2011; *Wang et al.*, 2012] to explain the coincidence of the magnetic anomalies and the coinciding characteristic albedo signatures (swirls). Our finding of a large positive

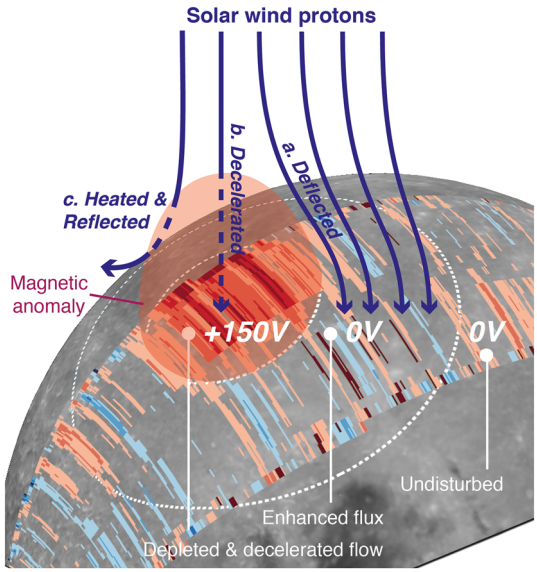

Figure 3. An illustration of the solar wind interaction with the lunar magnetic anomaly. Blue lines are solar wind proton streamlines modified by the interaction with the magnetic anomaly. The consequences of the incoming solar wind protons are (a) deflected and reached the enhanced region without a change in velocity, (b) decelerated inside the magnetic anomaly due to the potential structure of +150V and reached inside magnetic anomaly, or (c) heated and reflected in space before reaching the lunar surface.

electric potential structure all over the Gerasimovic anomaly supports the hypothesis of coinciding swirl formation.

[17] Despite its effects on the near-surface environment, this relatively large electrostatic potential above the magnetic anomaly does not pose any significant challenges for human and robotic activities on the Moon. The widely spread electric potential structure over the magnetized region suggests a relatively weak electric field. For example, assuming a 150V electrostatic potential along 200 km, the corresponding electric field is 0.8 mV/m, which is of the same order of the solar wind convection electric field at 1 AU. The vertical field could be stronger: If we assume 10 km, the electric field could be 15 mV/m. This is still not strong enough to influence the human and robotic activities directly, for example, discharging at the lunar surface. Therefore, a region under a magnetic anomaly still can be a good candidate site for landing and future exploration of the Moon. Secondary effects, such as dust levitation due to the electric field and its adsorption to any components [*Stubbs et al*., 2007], should be carefully assessed for robotic activities, but such effects are commonly observed everywhere on the Moon.

[18] **Acknowledgments.** This work was supported by funding from the Swedish National Space Board (SNSB) in Sweden. We thank the WIND/SWE team for providing the solar wind data.

References

Archinal, B. A., M. R. Rosiek, R. L. Kirk, and B. L. Redding (2005), "The united lunar control network 2005" (U.S. Geological Survey Open-File Report, 2006–1367.

Barabash, S., et al. (2009), Investigation of the solar wind-Moon interaction on board Chandrayaan-1 mission with the SARA experiment, *Curr. Sci.*, *96*(4), 526–532.

Barnes, A., P. Cassen, J. D. Mihalov, and A. Eviatar (1971), Permanent lunar surface magnetism and its deflection of the solar wind, *Science*, *172*(3984), 716–718.

Behrisch, R., and K. Wittmaack (1991), in *Sputtering by Particle Bombardment III*, edited by R. Behrisch and K. Wittmaack, 1–13 pp., Springer-Verlag, New York.

Colburn, D. S., R. G. Currie, J. D. Mihalov, and C. P. Sonett (1967), Diamagnetic solar-wind cavity discovered behind moon, *Science*, *158*(3804), 1040–1042.

Crider, D. H., and R. R. Vondrak (2002), Hydrogen migration to the lunar poles by solar wind bombardment of the moon, *Adv. Space Res.*, *30*(8), 1869–1874.

Dyal, P., C. W. Parkin, and W. D. Daily (1974), Magnetism and the interior of the Moon, *Rev. Geophys.*, *12*(4), 568–591.

Feldman, W. C., et al. (2000), Polar hydrogen deposits on the Moon, *J. Geophys. Res.*, *105*(E2), 4175–4195.

Freeman, J. W., M. A. Fenner, and H. K. Hills (1973), Electric potential of the Moon in the solar wind, *J. Geophys. Res.*, *78*, 4560–4567.

Freeman, Jr., J. W., and M. Ibrahim (1975), Lunar electric fields, surface potential and associated plasma sheaths, *The Moon*, *14*, 103–114.

Futaana, Y., S. Barabash, M. Holmström, and A. Bhardwaj (2006), Low energy neutral atoms imaging of the Moon, *Planet. Space Sci.*, *54*(2), 132–143.

Futaana, Y., et al. (2011), Exospheres and energetic neutral atoms of Mars, Venus and Titan, *Space Sci. Rev.*, *162*, 213–266.

Futaana, Y., et al. (2012), Empirical energy spectra of neutralized solar wind protons from the lunar regolith, *J. Geophys. Res.*, *117*, doi:10.1029/2011JE004019.

Garrick-Bethell, I., J. W. Head III, and C. M. Pieters (2011), Spectral properties, magnetic fields, and dust transport at lunar swirls, *Icarus*, *212*(2), 480–492.

Goldstein, B. E. (1974), Observations of electrons at the lunar surface, *J. Geophys. Res.*, *79*(1), 23–35.

Halekas, J. S., R. P. Lin, and D. L. Mitchell (2005), Large negative lunar surface potentials in sunlight and shadow, *Geophys. Res. Lett.*, *32*, doi:10.1029/2005GL022627.

Hood, L. L., P. J. Coleman, Jr., and D. E. Wilhelms (1979), Lunar nearside magnetic anomalies, *Proc. Lunar Planet. Sci. Conf.*, *10*, 2235–2257.

Lin, R. P., et al. (1998), Lunar surface magnetic field and their interaction with the solar wind: Results from lunar prospector, *Science*, *281*, 1480–1484.

Lue, C., et al. (2011), Strong influence of lunar crustal fields on the solar wind flow, *Geophys. Res. Lett.*, *38*(3), doi:10.1029/2010GL046215.

McComas, D. J., et al. (2009), Lunar backscatter and neutralization of the solar wind: First observations of neutral atoms from the Moon, *Geophys. Res. Lett.*, *36*(12), doi:10.1029/2009GL038794.

McComas, D. J., et al. (2012), The heliosphere's interstellar interaction: No bow shock. *Science*, *336*(6086), 1291–1293.

Niehus, H., W. Heiland, and E. Taglauer (1993), Low-energy ion scattering at surfaces, *Surf. Sci. Rep.*, *17*(4–5), 213–303.

Nitter, T., O. Havnes, and F. Melandso (1998), Levitation and dynamics of charged dust in the photoelectron sheath above surface in space, *J. Geophys. Res.*, *103*(A4), 6605–6620.

Němeček, Z., et al. (2011), Lunar dust grain charging by electron impact: Dependence of the surface potential on the grain size. *Ap. J.*, *738*, 1, doi:10.1088/0004-637X/738/1/14.

Purucker, M. E., and J. B. Nicholas (2010), Global spherical harmonic models of the internal magnetic field of the moon based on sequential and coestimation approaches, *J. Geophys. Res.*, *115*(E12), doi:10.1029/2010JE003650.

Rodríguez, M. D. F., et al. (2012), IBEX-Lo observations of energetic neutral hydrogen atoms originating from the lunar surface, *Planet. Space Sci.*, *60*(1), 297–303.

Saito, Y. et al. (2012), Simultaneous observation of the electron acceleration and ion deceleration over lunar magnetic anomalies, *Earth Planets Space*, *64*, 83–92.

Stubbs, T. J., R. R. Vondrak, and W. M. Farrell (2007), Impact of dust on lunar exploration, in *Dust in Planetary Systems*, SP-643, edited by H. Krüger, A. L. Graps, pp. 239–244, European Space Agency, Noordwijk, The Netherlands.

Stubbs, T. J., D. A. Glenar, W. M. Farrell, R. R. Vondrak, M. R. Collier, J. S. Halekas, and G. T. Delory (2011), On the role of dust in the lunar ionosphere, *Planet. Space Sci.*, *59*(13), 1659–1664.

Tsunakawa, H., et al. (2010), Lunar magnetic field observation and initial global mapping of lunar magnetic anomalies by MAP-LMAG onboard SELENE (Kaguya), *Space Sci. Rev.*, *154*(1-4), 219–251.

Vondrak, R. R. (1983), Lunar base activities and the lunar environment, in *2nd Conference on Lunar Bases and Space Activities*, (NASA, Johnson Space Center), 337–345 pp.

Vorburger, A., et al. (2012), Energetic neutral atom observations of magnetic anomalies on the lunar surface, *J. Geophys. Res.*, *117*(A7), doi:10.1029/2012JA017553.

Wang, X., M. Hornyi, and S. Robertson (2012), Characteristics of a plasma sheath in a magnetic dipole field: Implications to the solar wind interaction with the lunar magnetic anomalies, *J. Geophys. Res.*, *117*(A6), doi:10.1029/2012JA017635.

Whipple, E. C. (1981), Potentials of surfaces in space. *Rep. Prog. Phys.*, *44*, 1197–1250.

Wieser, M., et al. (2009), Extremely high reflection of solar wind protons as neutral hydrogen atoms from regolith in space, *Planet. Space Sci.*, *57*, 2132–2134.

Wieser, M., et al. (2010), First observation of a mini-magnetosphere above a lunar magnetic anomaly using energetic neutral atoms, *Geophys. Res. Lett.*, *37*(5), doi:10.1029/2009GL041721.